Journal of Applied Physics ARTICLE scitation.org/journal/jap

Decay of excess carriers in a two-defect model semiconductor: A time-resolved photoluminescence study

Cite as: J. Appl. Phys. **130**, 235702 (2021); doi: 10.1063/5.0065600
Submitted: 3 August 2021 · Accepted: 1 November 2021 ·
Published Online: 17 December 2021

Ashwin Hariharan,[a] Sascha Schäfer, and Stephan J. Heise

AFFILIATIONS

Ultrafast Nanoscale Dynamics, Institute of Physics, Carl von Ossietzky University of Oldenburg, Oldenburg, Germany

[a]**Author to whom correspondence should be addressed:** ashwin.hariharan@uni-oldenburg.de

ABSTRACT

The study of charge carrier decay dynamics in semiconductors plays an important role in determining various device properties, for example, the bulk minority carrier lifetime and the potential drop at interfaces. Time-resolved photoluminescence spectroscopy is an efficient technique to extract carrier decay time constants, with the simplest case being that of a mono-exponential decay controlled by a single type of recombination center. However, many modern materials often display multi-exponential decay behavior influenced by a broad distribution of defects. Utilizing $CuIn_{1-x}Ga_xSe_2$ as a reference system, we present a comprehensive and systematic theoretical study of the decay kinetics in a non-interacting two-defect-level system by using both the classical analytical approach developed by Hornbeck and Haynes and a homogeneous kinetic rate equation model solved numerically. We show how the trapping level's carrier capture cross-section symmetry factor and the initial injection level controls the parameter range for the agreement between these two approaches, analyzing the validity of multi-exponential fits for extracting the carrier lifetime. Further, we analytically and numerically demonstrate that information on the carrier recombination lifetime is contained in the fast time constant, whereas the agreement of the subsequent slow time constant with the analytical model depends on the energetic position of the defect level within the bandgap.

I. INTRODUCTION

Minority carrier lifetimes in semiconductors play an essential role in determining both material quality and device performance.[1,2] Time-resolved photoluminescence (TRPL) is the primary experimental tool to extract minority carrier lifetimes.[3–5] However, for many complex materials, such as $CuIn_{1-x}Ga_xSe_2$ (CIGS), it is well known that the bulk minority carrier recombination lifetime extracted using TRPL varies by several orders of magnitude, depending on the doping type, impurity concentration, and growth technique.[3,6–10] One of the main contributions to this variation is the presence of multiple defect levels distributed across the bandgap of the material,[11,12] which often leads to a multi-exponential luminescence decay[11,13] and requires a more detailed analysis of the underlying charge carrier kinetics, including the impact of trapping and recombination defects. Generally, the sensitivity of transient photoluminescence signals to trapping defects is comparatively low if the doping concentration is higher than the trap concentration.[14,15] However, for more complex materials, often high trapping densities are present, which modify or even dominate the charge carrier kinetics.

An analytical framework to study trapping effects was developed by Hornbeck and Haynes (H&H)[16,17] and was applied for the interpretation of transient photoconductivity (TPC) measurements in silicon. Since then, this model has been widely adopted, both for the interpretation of TPC[18,19] and of other experiments,[20–23] such as quasi steady-state photo conductance (QSSPC),[20] microwave detected photo conductance decay (MWPCD)[24,25] and carrier density imaging (CDI).[26] Extensions of the H&H model were developed for the description of the luminescence response from midgap radiative centers in wide bandgap materials.[27] Recently, the H&H model was applied to study the influence of trapping in TRPL experiments on CIGS,[28] for which trap concentrations are expected to be in the same range as the doping concentration.

In the H&H model, a strict distinction is being made between trapping and recombination defect centers. For more general defect

landscapes,[29–31] this central assumption is not always justified, rendering the application of the H&H model questionable, and a complete kinetic model is required, taking into account all transitions.

In the current study, we numerically analyze the effect of charge carrier trapping and recombination in a general two-defect-level system in comparison with the analytical H&H model for different combinations of defect levels. For the resulting charge carrier kinetics, we extract the expected TRPL signal recovering effects such as multi-exponential decay and signal saturation. The comparison of the analytical and numerical model provides a validity range for applying the H&H model to extract carrier lifetimes. Based on our findings, we provide guidelines for the interpretation of TRPL data in CIGS materials.

II. KINETICS OF CHARGE CARRIER RECOMBINATION AND TRAPPING

A. Statistical classification of defect levels

Within the Shockley–Read and Hall (SRH) picture, a monovalent defect allows for the capture and emission of electrons and holes.[32,33] The corresponding recombination, $R^{n,p}$, and generation rates, $G^{n,p}$, in thermal equilibrium are given by

$$R^n = c_n n(1\text{-}f_{DF})N_{DF}, \tag{1a}$$

$$G^n = e_n f_{DF} N_{DF}, \tag{1b}$$

$$R^p = c_p p f_{DF} N_{DF}, \tag{1c}$$

$$G^p = e_p(1\text{-}f_{DF})N_{DF}, \tag{1d}$$

in which $e_n = c_n n_1$ and $e_p = c_p p_1$ are the normalized emission rates for electrons and holes, respectively, n and p are the respective carrier densities, N_{DF} is the defect density, and f_{DF} is the thermal distribution function. n_1 and p_1 are auxiliary variables, defined by the electron and hole density for a system with the Fermi level at the defect-level energy. The capture coefficients $c_{n,p}$ are defined by $c_{n,p} = v_{th}\sigma_{n,p}$, in which v_{th} is the thermal carrier velocity and $\sigma_{n,p}$ are the capture cross sections (CCSs).

In general, a defect level can act as both a trapping and a recombination center, depending on its position within the bandgap and the ratio of the electron and hole capture cross sections, $\gamma = c_p/c_n$. Thereby, even when a defect level with a particular minority carrier CCS is placed in a recombination active zone, it might still produce considerable trapping effects, resulting in a different temporal evolution of minority and majority carrier densities.[34] Defect levels are generally classified as "shallow" defects, mainly performing trapping, and "deep" defects, facilitating recombination. Different criteria are being applied for this classification, including the ionization energy of the defect with respect to the thermal energy, or the size of the localized electron defect state relative to the lattice constant.[35,36] These classification schemes were mostly developed for conventional semiconductors such as silicon. In non-standard semiconductor materials, such as CIGS or CdTe, energy of the defect levels tend to lie far from the band edges, and intrinsic defects often result in doping and trapping, simultaneously.[37]

Based on the capture cross section symmetry, γ, we can introduce two characteristic energy levels distinguishing shallow and deep traps in perturbed p-type semiconductors, namely, the electron demarcation level[38] (E_{D_n}) and the quasi-Fermi level for trapped electrons[39] ($E_{QF}^{n_t}$), given by

$$E_{D_n} = E_c - E_{QF}^p + V_T \ln\left(\gamma \frac{N_V}{N_C}\right) \text{ and} \tag{2a}$$

$$E_{QF}^{n_t} = E_C + V_T \ln\left(\frac{n+\gamma p}{N_C}\right), \tag{2b}$$

in which E_c is the conduction band minimum, E_{QF}^p is the hole quasi-Fermi level, and $N_{C,V}$ is the band edge density of states in the conduction and valence band, respectively. V_T is the thermal energy at 300 K. Both reference levels not only depend on the intrinsic symmetry (γ) of the CCS but also on the excess carrier concentration, i.e., on the strength of the external perturbation, such as the incident optical fluence. In the limit of low injection conditions (implying that E_{QF}^p remains close to the equilibrium Fermi level E_F) and $\gamma \approx 1$, E_{D_n} and $E_{QF}^{n_t}$ are approximately equal.[40] With these reference levels, a defect is classified as a shallow trap if the defect energy is above $E_{QF}^{n_t}$. Defects with an energy below E_{D_n} act mainly as recombination centers. Defects with an energy in between $E_{QF}^{n_t}$ and E_{D_n} are considered to act as both trapping and recombination centers. A more detailed discussion on the classification of defects is given in the supplementary material.

B. Equations governing the decay from a two-defect-level system

In the following, we want to consider a semiconductor with two types of defects and a homogeneous optical excitation. Independently of their classification discussed above, we label the upper level as a trap defect (subscript "T") and the lower level as a recombination defect (subscript "R"). Using the transition rates defined by Eqs. (1)(a)–(1)(d) for each of the defect levels, we arrive at the following system of rate equations for the excess electron and hole density in the bands (Δn and Δp, respectively) and the excess density of populated defect levels (Δn_R and Δn_T),

$$\frac{d\Delta n}{dt} = G_{the}^n - (R_R^n - G_R^n) - (R_T^n - G_T^n) - R_{rad}^n, \tag{3a}$$

$$\frac{d\Delta p}{dt} = G_{the}^p - (R_R^p - G_R^p) - (R_T^p - G_T^p) - R_{rad}^p, \tag{3b}$$

$$\frac{d\Delta n_R}{dt} = (R_R^n - G_R^n) - (R_R^p - G_R^p), \tag{4a}$$

$$\frac{d\Delta n_T}{dt} = (R_T^n - G_T^n) - (R_T^p - G_T^p). \tag{4b}$$

Furthermore, due to charge neutrality, the following equation holds

$$\Delta p - \Delta n - \Delta n_R - \Delta n_T = 0. \tag{4c}$$

In addition to the defect-related transitions, Eqs. (3) and (4) contain additional terms $G^{n,p}_{the}$ and $R^{n,p}_{rad}$, describing the thermally induced generation of carriers and the band-to-band radiative recombination, respectively. A graphical representation of the individual transitions is given in Fig. 1(a).

C. Hornbeck–Haynes model

Generally, the set of differential equations defined by Eqs. (3) and (4) is not analytically solvable and further simplifications are often employed. In the H&H model,[16,17] originally developed for doped silicon, the emission of carriers from the lower energy defect, i.e., the recombination center, is ignored. Furthermore, the upper energy level is considered to exclusively act as a trapping center with no recombination activity. A graphical representation of the modified allowed transitions for a p-type semiconductor is given in Fig. 1(b). Analytically, the following approximate substitutions are applied (see the supplemental material for details),

$$R^n_R - G^n_R = \frac{n - n_0}{\tau_n^{R_0}}, \tag{5}$$

in which $\tau_n^{R_0}$ is the SRH lifetime (i.e., the minority carrier lifetime), given as $(c_n^R N_R)^{-1}$, and governed by the capture rate and the concentration of recombination defects.[32,33]

Utilizing the charge neutrality condition and ignoring band-to-band contributions, Eqs. (3) and (4) can be rewritten in explicit form as[34]

$$\frac{d\Delta n}{dt} = -\left(\frac{1}{\tau_n^{R_0}} + \frac{1}{\tau_n^{T_0}}\right)\Delta n + \frac{1}{\tau_n^{e_T}}\Delta n_T + c_n^T \Delta n \Delta n_T, \tag{6a}$$

$$\frac{d\Delta n_T}{dt} = -\frac{1}{\tau_n^{e_T}}\Delta n_T + \frac{1}{\tau_n^{T_0}}\Delta n - c_n^T \Delta n_T \Delta n. \tag{6b}$$

Here, $\tau_n^{T_0} = (c_n^T N_T)^{-1}$ and $\tau_n^{e_T} = (c_n^T(n_0 + n_1))^{-1}$ are the capture and emission time constants for the trap level. (The complete system of equations also considering the hole dynamics is provided in the supplementary material.) For low injection conditions and for traps located above $E_{QF}^{n_t}$ or small c_n^T, the nonlinear terms containing $\Delta n \cdot \Delta n_T$ can be ignored, resulting in a simple biexponential decay of the excess free carrier density,[28] Δn. The corresponding time constants are obtained as

$$\tau_{1,2} = \frac{2}{\omega_1 \pm \omega_2}, \tag{7}$$

with

$$\omega_1 = \left(\frac{1}{\tau_n^{R_0}} + \frac{1}{\tau_n^{T_0}} + \frac{1}{\tau_n^{e_T}}\right) \text{ and } \omega_2 = \sqrt{\omega_1^2 - \frac{4}{\tau_n^{R_0}\tau_n^{e_T}}}.$$

In these limits, information on the carrier lifetime may be gained by a biexponential fit of the TRPL decay. Further extensions of the H&H model, also partially including recombination from the trap level, is provided in the appendix of Ref. 16.

III. METHODOLOGY

To assess the range of applicability of the H&H model, we compare the biexponential analytical results using Eq. (7) with numerical solutions of the full set of rate equations [Eqs. (3) and (4)]. As an example, we consider carrier kinetics in a homogeneously excited p-type CIGS layer. Since the reported data on the energy and carrier cross section of relevant defects in this material system vary considerably (see the supplemental material for a literature review and for additional material parameters used), we chose a fixed energy for the recombination center at the intrinsic Fermi level (chosen at 623 meV above the valence band edge) and a range of energies for the trapping defect level.

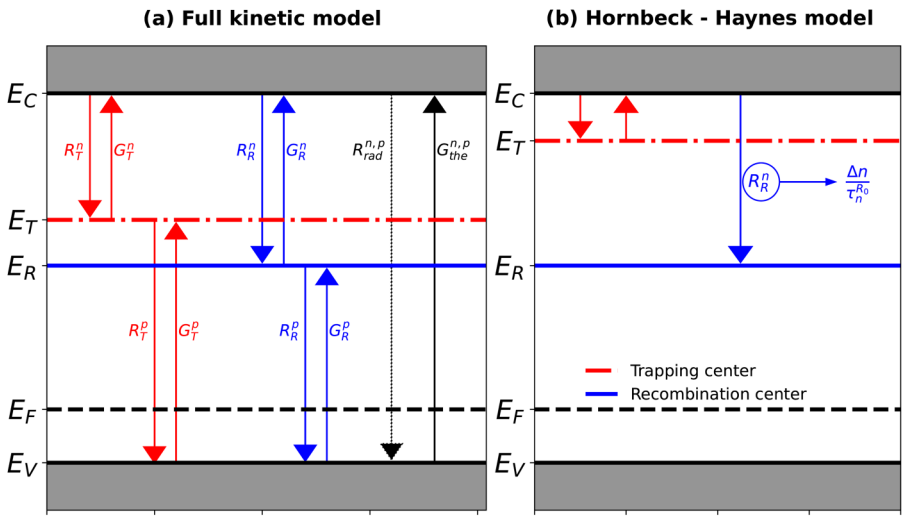

FIG. 1. Two-defect-level system under two approaches in a p-type semiconductor. The thermal transitions for both defect levels and the bands are indicated by arrows from an electron's perspective. (a) The general two-defect-level model where both defect states could be present anywhere in the bandgap. (b) The Hornbeck–Haynes model where the trap state should lie at or above the trapped electrons quasi-Fermi level and the recombination center should be present near the midgap. A donor-like trap and an acceptor-like recombination center are assumed.

Four defect energy levels are considered in the top half of the bandgap. Their effect on the decay kinetics depends on the initial defect (trap center) occupation function (f_T) (i.e., their relative position w.r.t $E_{QF}^{n_t}$ and E_{D_n}), parametrized by the initial carrier density (Δn_o) and the symmetry factor (γ_T and γ_R). The four cases based on these two parameters are presented in Fig. 2.

Furthermore, we choose N_R as 4×10^{15} cm^{-3}, σ_n^R as 5×10^{-15} cm^2, and a symmetry factor of γ_R as unity. N_T was also kept constant at 8.0×10^{15} cm^{-3} with two values of σ_n^T at 5×10^{-15} and 5×10^{-16} cm^2. The recombination center and trapping defect densities are selected such that their values are below and above the critical defect density, respectively, to induce trapping effects.[41] With these parameters and a thermal velocity of 1×10^7 cm/s, the minority carrier lifetime $\tau_n^{R_0}$ is obtained as 5 ns.

To allow for a direct comparison to an experimental observable, we calculate for each case the temporal evolution of the photoluminescence intensity, given as

$$I_{PL} = B_{BTB} \times [(n_0 + \Delta n)(p_0 + \Delta p) - n_0 p_0], \tag{8}$$

which directly scales with the excess electron concentration in the p-type system considered here. Here, B_{BTB} is the radiative recombination coefficient.

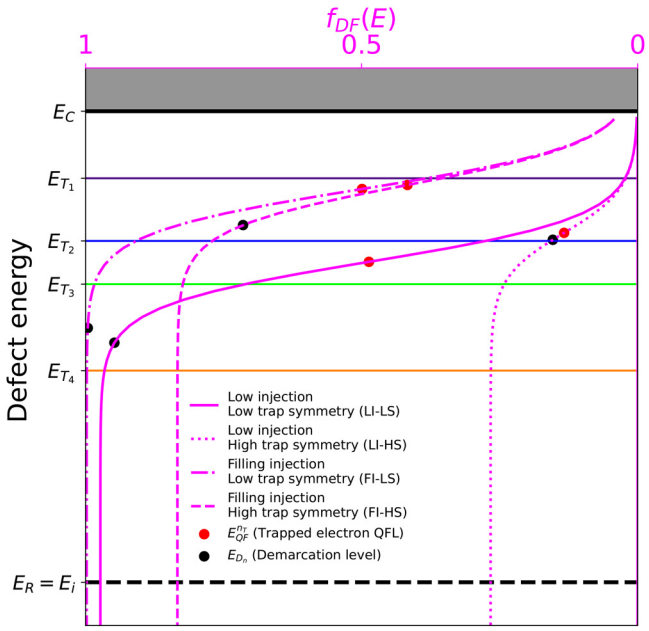

FIG. 2. Defect energy level diagram for traps and recombination center. The energy level position for the traps are $E_{T_1} = 3V_T$, $E_{T_2} = 150$ meV, $E_{T_3} = 200$ meV, and $E_{T_4} = 300$ meV below E_C. The magenta plot and scale represent the steady-state trap level occupation function to signify the characteristic energy level positions for the four different cases analyzed in this study: (a) (LI-LS) $\Delta n = 7.5 \times 10^{14}$ cm^{-3}, $\gamma_T = 0.001$. (b) (LI-HS) $\Delta n = 7.5 \times 10^{14}$ cm^{-3}, $\gamma_T = 0.1$. (c) (FI-HS) $\Delta n = 2 \times 10^{16}$ cm^{-3}, $\gamma_T = 0.1$. (d) (FI-LS) $\Delta n = 2 \times 10^{16}$ cm^{-3}, $\gamma_T = 0.001$. The energies of the demarcation level and the TQFL are indicated by dots.

We note that most of the interesting features in the carrier kinetics are visible if the capture cross sections of trap and recombination center are comparable. The results for the case $\sigma_n^T < \sigma_n^R$ are provided in the supplemental material for comparison.

With the employed material parameters and injection levels, nonlinear effects in the radiative band-to-band recombination are still negligible, as Δn is equal or smaller than the doping level.

For obtaining a numerical solution of the full kinetic model [Eqs. (3) and (4)], we utilized a backward differentiation formula (BDF) approach as implemented in the Python Scipy package using a temporal delta-like function for the carrier injection.[42]

For evaluating the impact of nonhomogeneous carrier injection, we additionally employed a finite volume in space and finite difference in time approach, as implemented in the TCAD Sentaurus software suite. The corresponding results are detailed in the supplemental material.

IV. RESULTS AND DISCUSSION

A. Carrier decay at low injection and low trap symmetry

We start the discussion by first considering conditions for which the H&H model is most applicable, i.e., at a low carrier injection [reducing the influence of the nonlinear term in Eq. (6)] and at low trap symmetry (resulting in minimum interaction of the trap level with the valence band).

The results for the temporal evolution of the excess carrier density, and, thus, the PL intensity, is shown in Fig. 3 for different trap level energies. As expected for the chosen conditions, the H&H model (broken curves) overall provides an excellent approximation to the full rate equation (solid curves).

The extracted instantaneous PL lifetime, defined as[43,44] $\tau_{eff}(t) \equiv -1/(d \ln(I_{norm}(t))/dt)$, is given in the inset of Fig. 3, where $I_{norm} \equiv I_{PL}/\max(I_{PL})$. We further consider $\tau_{eff}(t)$ in the two limiting cases: $\tau_{eff}^1 \equiv \tau_{eff}(t \to 0)$ and $\tau_{eff}^2 \equiv \tau_{eff}(t \to \infty)$. As visible in the inset, the biexponential behavior of the H&H model is well reproduced in the full rate equation approach. Physically, the fast time constant of the biexponential, $\tau_{eff}^1 = (1/\tau_n^{R_0} + 1/\tau_n^{T_0})^{-1}$, is governed by the parallel capture process by both defect levels, independent of the emission time constant $\tau_n^{e_T}$.

The dynamics of the slower time constant (τ_2) is primarily controlled by the emission of the trapped electrons. For trap defect levels above $E_{QF}^{n_t}$ and for trap level densities smaller than n_1, τ_2 approaches the recombination time $\tau_n^{R_0}$, since the emission from the trap level is fast compared with the recombination, i.e., $\tau_n^{e_T} < \tau_n^{R_0}$ and $\tau_n^{e_T} < \tau_n^{T_0}$. For the current case, this limiting scenario is realized for E_{T_1} for which n_1 equals 3.2×10^{16} cm^{-3}.

Already for a trap level at energy E_{T_2}, τ_2 starts to increase, approaching a multiple trapping regime before recombination occurs, yielding a time constant $\tau_n^{e_T}(1 + \tau_n^{R_0}/\tau_n^{T_0})$ (see the supplemental material for further details).

For trap level energies close to or below the demarcation energy (E_{T_3} and E_{T_4}), τ_2 further increases and now exhibits a marked contrast between the H&H and the full kinetic model, as visible in the inset of Fig. 3. This discrepancy in the H&H model is caused by ignoring the direct recombination via the trap level. Therefore, in the H&H model, a trapped electron can only

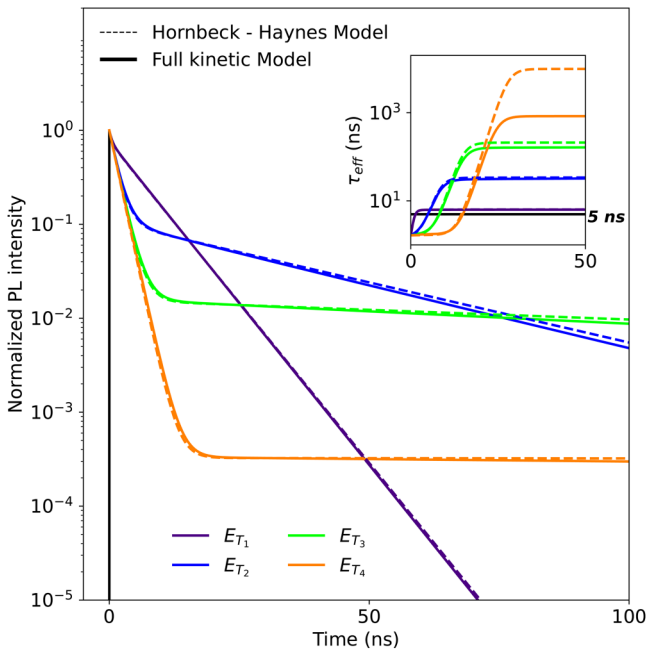

FIG. 3. Normalized PL intensity decay for low injection and low trap symmetry. The main plot represents calculated solutions using the two approaches of the full kinetic model (solid lines) and the HH model (dashed lines). The decays are shown for four different energy levels of the trapping defect (color-coded). The inset plot represents the absolute value of the slope. Here, a 5 ns reference horizontal curve would represent a mono-exponential decay in the main plot for bulk lifetime. For the case considered here, the defect quasi-Fermi energy $E_{QF}^{n_t}$ and the demarcation level E_{D_n} are at 174 and 268 meV, respectively, relative to the conduction band minimum. Therefore, defect levels at energies E_{T_1} and E_{T_2} would be considered as shallow traps, a level at E_{T_4} as a deep trap, and E_{T_3} is the in transition zone.

recombine by initial emission from the trap level and subsequent capture by a recombination center.

The current case demonstrates that minority carrier lifetimes can be extracted from time-resolved photoluminescence experiments using the simple H&H model, if trap levels are within about 300 meV from the conduction band and γ_T is low. Considering reported defect levels in CIGS as an example (see the supplemental material), the criterion regarding the defect energy seems to be fulfilled, but trap symmetry parameters have not yet been established.

B. Carrier decay at low injection and high trap symmetry

Even though defects in CIGS are mostly multivalent[45] and highly asymmetric γ-values are expected from Coulomb arguments, recent microscopic simulations in a related system have demonstrated that also in these cases, more symmetric γ-values, i.e., $\gamma \approx 1$, can occur.[46] In order to gauge the impact of the symmetry factor of the trap level, we simulated the normalized photoluminescence intensity for $\gamma_T = 0.1$ within the full kinetic model and compare it with the analytical H&H model. The results are plotted for a continuum of trap energies in a color-coded map in Figs. 4(a) and 4(b). Sections of the map for selected trap energies are shown in Fig. 4(c).

As expected, for the fast decay (τ_1), which is dominated by the interaction of the conduction band with the trap level, the ratio of the electron and hole capture cross sections of the recombination center does not play any role, resulting in similar kinetics as in Fig. 3.

In contrast to Sec. IV A, we now observe for all four energy levels a significant difference in the slow time constant (τ_2) between the approximate H&H model and the full kinetic model. The deviations observed are related to a larger recombination activity now directly occurring via the trap level.

As visible from a comparison of the color maps, the energy region for which the H&H model remains (approximately) applicable is now reduced to a narrow interval close to the conduction band minimum, which, however, falls outside of the Boltzmann limit of the Fermi–Dirac distribution assumed in Eq. (1).

Furthermore, in the color map, the breakdown of the H&H model for deep traps, which also act as recombination centers, is clearly visible.

Overall, also for high trap symmetries, the minority carrier lifetime can be, in principle, be extracted from the fast component of the decay. However, this component is not clearly discernible due to its small amplitude, as visible in Fig. 4(c), for example, for the defect energy at (E_{T_1}).

C. Carrier decay at the trap-filling injection

In Sec. IV C, we address recombination dynamics in the high-injection regime, which is often relevant for time-resolved PL experiments. Under such conditions, the recombination centers can become saturated, producing a marked difference in the free electron dynamics as compared with the predictions of the H&H model. Figure 5 shows the PL decay [Fig. 5(a)] and the reduction of carrier concentration over time [Fig. 5(b)] evaluated for the case of high symmetry, $\gamma_T = 0.1$, and a trap-filling injection level of 2×10^{16} cm^{-3} (i.e., at a value higher than the trap and recombination center density).

Comparing the PL slope in Figs. 5(a) and 4(c), it is apparent that the higher injection level does not significantly affect recombination dynamics at later times (corresponding to τ_2) since at these times the remaining carrier density is comparable to the initial density at low injection. At early times, the full kinetic model yields a super-linear carrier decay up to 20 ns if deep trap levels are considered (e.g., E_{T_4} in the present case). This behavior is caused by a saturation of the recombination defect.[15,47–50]

For deep traps and ignoring the emission terms in the general two-level model (i.e., setting $G_{R,T}^n = 0$), the rate equation for the excess carrier density reduces to

$$\frac{d\Delta n}{dt} = -\left(\frac{1-\Delta f_R}{\tau_n^{R_0}} + \frac{1-\Delta f_T}{\tau_n^{T_0}}\right)\Delta n, \tag{9}$$

in which Δf_R and Δf_T are the time-dependent defect occupation functions of the recombination and the trap level, respectively. Thus, for high defect occupation $\Delta f_{R,T}$, a reduction of the effective parallel capture process is observed. Considering the effective time

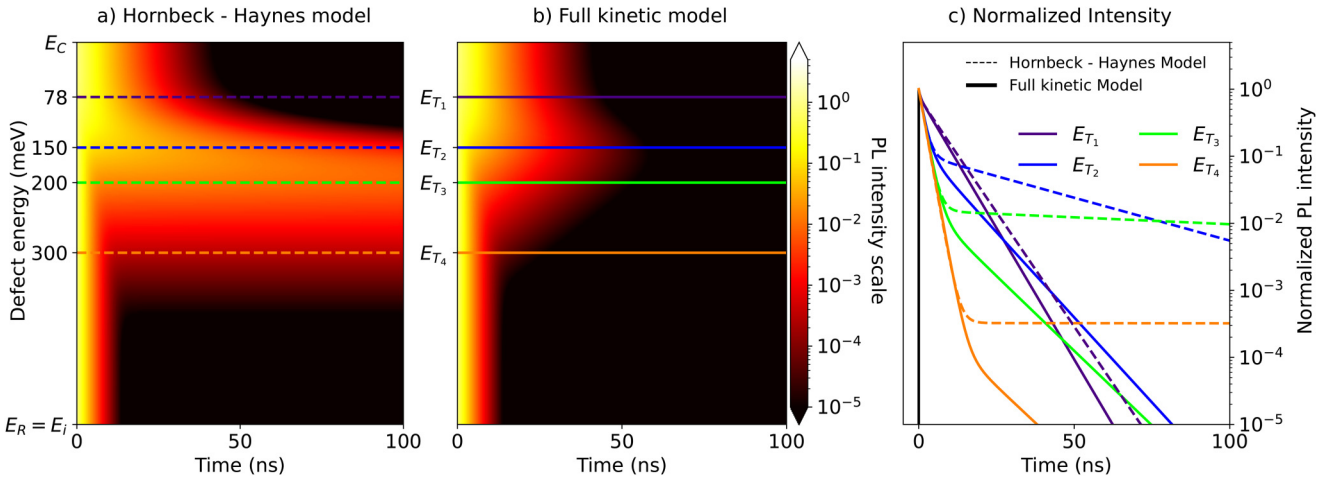

FIG. 4. Color map and normalized intensity decay for low injection and high trap symmetry. The color map represents the normalized intensity decay for a continuous distribution of defects in the top half of the bandgap using (a) the Hornbeck–Haynes model and (b) full kinetic model. Plot (c) represents the normalized intensity at the four defect levels under discussion. In this case, $E_{QF}^{n_t}$ and E_{D_n} become closer in magnitude at 141 and 149 meV, respectively, and consequently, E_{T_2} is almost equivalent to the demarcation level. Further, E_{T_1} is a shallow trap, while E_{T_3} and E_{T_4} are deep traps.

constant [Fig. 5(a), inset], a maximum value of 3.35 ns is observed at 2.8 ns for the case of a trap level at E_{T_4}, which is higher than the parallel capture time of 2.5 ns, when all defects are empty. The corresponding excess occupation values at this time are $\Delta f_T = 0.66$ and $\Delta f_R = 0.20$, respectively.

An explicit expression for $\Delta f_{T,R}$ using the steady-state occupation function under the quasi-neutrality condition was given for an n-type system, resulting in a decoupled nonlinear carrier rate equation at moderate injection levels.[48] Applying steady-state occupation functions may not be valid for defect concentrations higher than a critical concentration, which causes considerable trapping effects.[41] To provide a quantitative comparison in a more general scenario, the steady-state approach from Ref. 48 is extended to a two-defect-level system (see the supplemental material), while retaining the coupling between free carriers. In Fig. 5(b), the results of this approximate approach (cyan curve) are compared with the general recombination kinetics model with (orange curve) and without (red curve) including the emission terms. As a reference, additionally, the carrier density decay (black curves) with no trap levels present is shown. In general, the approximate steady-state approach describes the bulging behavior well. At early times, free carriers are not fully equilibrated with the defect levels and the steady-state approach overestimates the defect excess occupations. Therefore, the approximated approach predicts a slightly slower carrier decay.

Finally, we discuss the high-injection behavior at low symmetry. As visible from Figs. 5(c) and 5(d), under these conditions, significant super-linear decay behavior is observed. For the chosen injection density, the density of the trap levels is still sufficient to store carriers for time scales larger than the recombination time through the recombination centers. Therefore, the density of non-occupied recombination centers is no longer the bottleneck for the carrier decay kinetics. At even higher injection levels, we again observe a super-linear decay behavior like for the high-symmetry case discussed above.

Thus, with a more concrete information of the defect concentration and its energetic position, in principle, one can gain knowledge about the nature of symmetry of the trap level in the material under trap-filling injection conditions.

All of the above information can be summarized diagrammatically in Fig. 6, in which the limiting cases for the effective time constant values (τ_{eff}^1 and τ_{eff}^2) for all the trap levels located in the top half of the bandgap are provided for $\sigma_n^T = \sigma_n^R$. The analyzed defect cases are also marked accordingly for comparison. (A similar figure for $\sigma_n^T < \sigma_n^R$ is provided in the supplemental material.) Furthermore, we have considered the temperature dependence of the decay kinetics (close to room temperature) for $\sigma_n^T = \sigma_n^R$ in the supplementary material.

D. Implications for the interpretation of TRPL data in CIGS

In this section, we compare our analysis with the existing experimental data in the corresponding literature[3,5–10,13,52–79] and provide some interpretations for TRPL measurements in the framework of the two-defect-level model presented here.

In several publications on CIGS TRPL, a mono-exponential decay has been observed,[3,5–7,13,51–53,56,60,64–66,70–73,78,79] which could result from the following experimental and material-specific circumstances: (a) in the case of a deep trap, the experimentally retrieved curve would correspond to the parallel capture time (τ_{eff}^1 cf. Fig. 3 orange curve). At an increased injection level, a bulging behavior should be visible,[66] particularly for symmetric traps (cf. Fig. 5). (b) A quasi-mono-exponential decay is also possible when the trap level is very shallow such that the

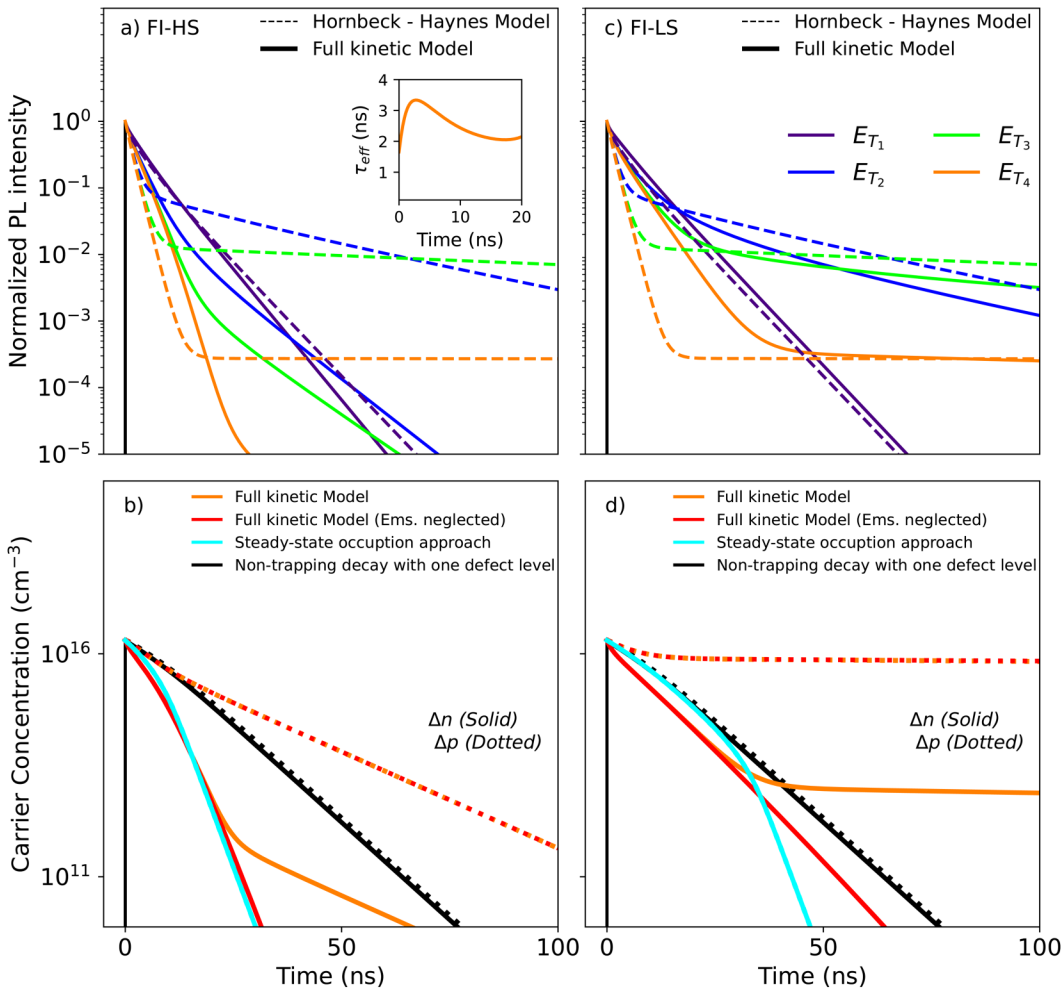

FIG. 5. Normalized decays for trap-filling injection: (a) and (b) represent the high electron trap symmetry kinetics, while (c) and (d) represent the kinetics under low trap symmetry. (a) and (c) represent the normalized PL intensity decay curves for the four trap levels specified in Fig. 2. (b) and (d) represent the carrier concentration decays for the deep trap (E_{T_4}) using different approaches (described in the text). A reference carrier concentration decay for a non-trapping midgap defect with a 5 ns time constant is shown in black. For the FI-HS case, $E_{OF}^{n_t}$t lies at 85 meV and E_{D_n} at 131 meV from the conduction band minimum. Thus, except for E_{T_1} (shallow trap), all traps are deep. For the FI-LS case, only E_{D_n} changes its position to 251 meV, thus bringing E_{T_2} and E_{T_3} to the transition region.

measured decay directly reflects the carrier lifetime. In such a case, the injection level dependence follows the standard SRH theory. (c) In addition, the temporal resolution of the TRPL setup might be insufficient to detect the initial fast drop in PL intensity during trapping.[28,63,69] In such a case as well, only a single exponential is measurable, the slower time constant τ_2 is retrieved, and low temperature TRPL might be helpful to shift the trapping time constant within an experimentally accessible time resolution window (see the supplemental material for the numerical solutions of this case under two injection levels). One experimental observable pointing to fast trapping is a decreased peak PL intensity as compared with the cases (a) and (b).

For the measured PL decay to be observed as a biexponential, as in another broad number of publications,[8,9,54,55,57–59,61,62,67,68,74–77] both time constants need to be detectable within the time resolution of the experiments (typically > 1 ns), and the amplitude of both exponential components needs to be comparable. Following S3.3 in the supplemental material, the second requirement is fulfilled if the emission rate $\tau_n^{e_T}$ is comparable to the parallel capture rate τ_{eff}^{1}. For the material parameters considered here, this condition is adopted for trap levels varying between 90 and 260 meV, depending on the symmetry factor and injection level. For the case of pronounced biexponential behavior, the following general trends are observed: (a) for symmetric traps, increasing the injection level does merely result in a linear scaling of PL intensity without significant change in the time constants, as visible in the LI-HS and FI-HS curves in Fig. 6. (b) For asymmetric traps, with increasing injection, the faster time constant increases and the slower time

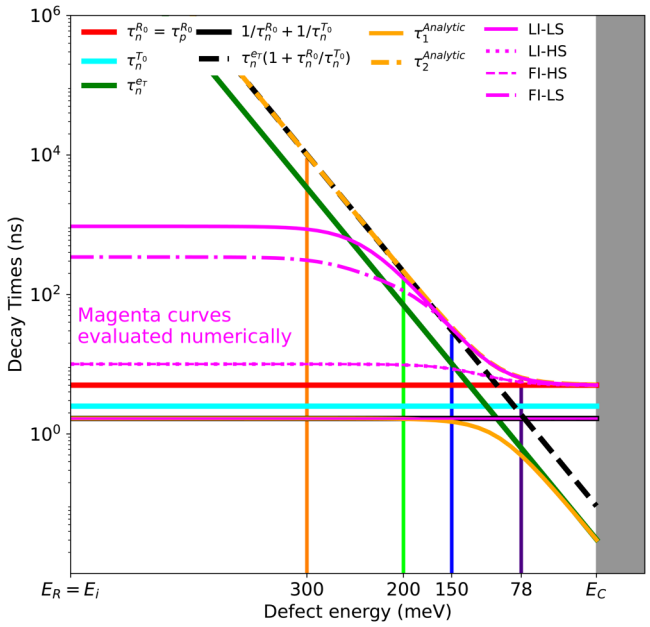

FIG. 6. Time constant diagram for all investigated cases as a function of trapping defect energy in the top half of the bandgap. τ^1_{eff} is similar for all cases and is plotted on the parallel capture time. $\tau_n^{E_T}$ (green line) is known as a single trapping time, while $\tau_n^{e_T}(1+\tau_n^{R_0}/\tau_n^{T_0})$ (black—dashed) is known as the multiple trapping time. $\tau^{Analytic}_{1,2}$ represents the time constant from the analytical model [Eq. (7)]. Magenta lines represent the numerically evaluated curves using the full kinetic model for each case. As visible, the numerically evaluated τ^1_{eff} for all cases is similar [superimposed on the parallel capture (black—solid) time constant].

constant decreases, as shown in the corresponding LI-LS and FI-LS.

As a concluding remark, the broad range of TRPL results reported for the CIGS sample seems to imply that the different material preparation and processing parameters employed in these studies change not only the defect concentration but also the dominant defect types. Such a diverse behavior renders TRPL a very useful technique for its characterization but with great challenges in terms of a proper microscopic interpretation.

V. CONCLUSION

In conclusion, we considered a non-interacting two-defect-level system with monovalent transitions both within a full rate-equation model and within the approximate Hornbeck & Haynes analytical approach. In the four parametric cases considered, based on injection level and symmetry factor of the capture cross section, we observe that in the low injection regime the fast time constant, governed by the free electron dynamics, is independent of the trap energy level and agrees well with the analytical effective time constant expression. In the trap-filling injection regime, saturation effects are visible in the full rate-equation model, which are modulated by the excess defect occupation function, parametrized by the injection level and symmetry factor. The slower time constant, governed by the trapped electron dynamics, shows no dependence on the injection level for high trap symmetry but a weak dependence for the low trap symmetry case. However, the agreement with the analytical effective time constant expression depends on the trap energy level with respect to the trapped quasi-Fermi level (TQFL) position of the corresponding trap.

One important aspect of the carrier dynamics in such systems entails its impact on the photovoltaic device properties. In a simple one-defect model, the dynamics can be described by a simple minority carrier lifetime with direct consequences for the open-circuit voltage and carrier collection efficiency of a particular device. In the case of two-defect types with varying degrees of recombination and trapping activity, a more complicated physical picture emerges, in which purely trapping defects affect both current collection efficiency and open-circuit voltage in different ways. However, recombination defects result in a reduction of both quantities. Therefore, photovoltaic absorbers with a broad variety of defects are not sufficiently characterized by a simple minority carrier lifetime, and, therefore, more elaborate theoretical models and accompanying analysis of, for example, time-resolved photoluminescence transients might facilitate the future optimization of these more complex absorber materials.

SUPPLEMENTARY MATERIAL

See the supplementary material for additional information on the defect classification, full rate equation governing the kinetics, the literature of survey of relevant parameters, TCAD Sentaurus results for inhomogeneous generation effects, temperature effects, and auxiliary results.

ACKNOWLEDGMENTS

This work was supported by the German Ministry of Economy and Energy (Grant No. 0324297F, "OptiCIGS-II"); and their support is hereby gratefully acknowledged.

AUTHOR DECLARATIONS

Conflict of Interest

The authors have no conflicts to disclose.

DATA AVAILABILITY

The data that support the findings of this study are available from the corresponding author upon reasonable request.

NOMENCLATURE

Δf_{DF}	Non-equilibrium occupation function of a defect level (—)
Δn	Excess electron concentration (cm^{-3})
Δp	Excess hole concentration (cm^{-3})
B_{BTB}	Radiative recombination coefficient ($cm^3 s^{-1}$)
c_n	Electron capture coefficient ($cm^3 s^{-1}$)
c_p	Hole capture coefficient ($cm^3 s^{-1}$)
E^p_{QF}	Hole quasi-Fermi level (eV)
E_F	Equilibrium Fermi level (eV)
e_p	Hole emission rate (s^{-1})

e_n	Electron emission rate (s^{-1})
f_{DF_0}	Equilibrium occupation function of a defect level (—)
G_{the}	Band-to-band thermal generation rate ($cm^{-3}s^{-1}$)
N_C	CBM density of state (cm^{-3})
N_R	Total recombination center concentration (cm^{-3})
N_T	Total trap concentration (cm^{-3})
N_V	VBM density of state (cm^{-3})
n_1	Thermal electron density when the Fermi level is at the energy of a non-degenerate trap (cm^{-3})
n_i	Intrinsic carrier concentration (cm^{-3})
n_o	Equilibrium electron concentration (cm^{-3})
n_{R_0}	Equilibrium recombination center concentration (cm^{-3})
n_{T_0}	Equilibrium trap concentration (cm^{-3})
Δn_T	Excess occupied trap concentration (cm^{-3})
R_{rad}	Band-to-band radiative recombination rate ($cm^{-3}s^{-1}$)
p_o	Equilibrium hole concentration (cm^{-3})
p_1	Thermal hole density when the Fermi level is at the energy of a non-degenerate trap (cm^{-3})
V_T	Thermal energy at 300 K (eV)

REFERENCES

[1]R. K. Ahrenkiel and M. S. Lundstrom, *Minority Carriers in III-V Semiconductors: Physics and Applications*, Semiconductor and Semimetals Vol 39 (Academic Press Inc., 1993).
[2]D. K. Schröder, IEEE Trans. Electron Devices **44**, 160 (1997).
[3]W. K. Metzger, I. L. Repins, M. Romero, P. Dippo, M. Contreras, R. Noufi, and D. Levi, Thin Solid Films **517**, 2360 (2009).
[4]J. F. L. Salas, S. J. Heise, M. Richter, V. Gerliz, M. S. Hammer, J. Ohland, and I. Hammer-Riedel, Thin Solid Films **633**, 40 (2017).
[5]T. P. Weiss, B. Bissig, T. Feurer, R. Carron, S. Buecheler, and A. N. Tiwari, "Bulk and surface recombination properties in thin film semiconductors with different surface treatments from time-resolved photoluminescence measurements," Sci. Rep. **9**, 5385 (2019).
[6]W. K. Metzger, I. L. Repins, and M. A. Contreras, Appl. Phys. Lett. **93**, 022110 (2008).
[7]B. M. Keyes, P. Dippo, W. K. Metzger, J. AbuShama, and R. Noufi, J. Appl. Phys. **94**, 5584 (2003).
[8]S. Shirakata and T. Nakada, Thin Solid Films **515**, 6151 (2007).
[9]S. I. Shimakawa, K. Kitani, S. Hayashi, T. Satoh, Y. Hashimoto, Y. Takahashi, and T. Negami, Phys. Status Solidi A **203**, 2630 (2006).
[10]R. Scheer, A. Pérez-Rodríguez, and W. K. Metzger, Prog. Photovoltaics Res. Appl. **18**, 467 (2010).
[11]S. Siebentritt, M. Igalson, C. Persson, and S. Lany, Prog. Photovoltaics Res. Appl. **18**, 390 (2010).
[12]A. Krysztopa, M. Igalson, L. Gütay, J. K. Larsen, and Y. Aida, Thin Solid Films **535**, 366 (2013).
[13]A. Redinger, S. Levcenko, C. J. Hages, D. Greiner, C. A. Kaufmann, and T. Unold, Appl. Phys. Lett. **110**, 122104 (2017).
[14]F. D. Heinz, W. Warta, and M. C. Schubert, Sol. Energy Mater. Sol. Cells **158**, 107 (2016).
[15]R. K. Ahrenkiel, N. Call, S. W. Johnston, and W. K. Metzger, Sol. Energy Mater. Sol. Cells **94**, 2197 (2010).
[16]J. A. Hornbeck and J. R. Haynes, Phys. Rev. **97**, 311 (1955).
[17]J. R. Haynes and J. A. Hornbeck, "Trapping of minority carriers in silicon. II. *n*-type silicon," Phys. Rev. **100**, 606–615 (1955).
[18]Y. Hu, H. Schøn, O. Nielsen, E. Johannes Øvrelid, and L. Arnberg, "Investigating minority carrier trapping in n-type Cz silicon by transient photoconductance measurements," J. Appl. Phys. **111**, 053101 (2012).
[19]Y. Zhu, M. K. Juhl, G. Coletti, and Z. Hameiri, IEEE J. Photovoltaics **9**, 652 (2019).
[20]D. Macdonald and A. Cuevas, Appl. Phys. Lett. **74**, 1710 (1999).
[21]R. A. Bardos, T. Trupke, M. C. Schubert, and T. Roth, Appl. Phys. Lett. **88**, 053504 (2006).
[22]N. Khelifati, D. Bouhafs, M. Boumaour, S. E. H. Abaidia, and B. Palahouane, Mater. Sci. Semicond. Process. **15**, 56 (2012).
[23]Y. Jung, K. H. Min, S. Bae, Y. Kang, D. Kim, and H.-S. Lee, Energies **13**, 5783 (2020).
[24]K. Lauer, A. Laades, H. Übensee, H. Metzner, and A. Lawerenz, J. Appl. Phys. **104**, 104503 (2008).
[25]R. Guo, W. Jie, N. Wang, G. Zha, Y. Xu, T. Wang, and X. Fu, "Influence of deep level defects on carrier lifetime in CdZnTe:In," J. Appl. Phys. **117**, 094502 (2015).
[26]M. C. Schubert, S. Riepe, S. Bermejo, and W. Warta, J. Appl. Phys. **99**, 114908 (2006).
[27]J. M. Dishman, Phys. Rev. B **6**, 1337 (1972).
[28]M. Maiberg, T. Hölscher, S. Zahedi-Azad, and R. Scheer, "Theoretical study of time-resolved luminescence in semiconductors. III. Trap states in the band gap," J. Appl. Phys. **118**, 105701 (2015).
[29]K. C. Nomura and J. S. Blakemore, Phys. Reve. **112**, 1607–1615 (1958).
[30]K. C. Nomura and J. S. Blakemore, Phys. Rev. **121**, 734–740 (1961).
[31]B. Das, I. Aguilera, U. Rau, and T. Kirchartz, Phys. Rev. Mater. **4**, 024602 (2020).
[32]R. N. Hall, Phys. Rev. **87**, 387 (1952).
[33]W. Shockley and W. T. Read, Phys. Rev. **87**, 835 (1952).
[34]J. S. Blakemore, *Semiconductor Statistics* (Pergamon Press, 1962).
[35]C. T. Sah, *Fundamentals of Solid-State Electronics* (World Scientific Publishing Co. Pte. Lfd, 1991).
[36]A. Alkauskas, M. D. McCluskey, and C. G. Van De Walle, J. Appl. Phys. **119**, 181101 (2016).
[37]K. K. Chin, "Dual roles of doping and trapping of semiconductor defect levels and their ramification to thin film photovoltaics," J. Appl. Phys. **111**, 104509 (2012).
[38]A. Rose, Phys. Rev. **97**, 322 (1955).
[39]J. G. Simmons and G. W. Taylor, Phys. Rev. B **4**, 502 (1971).
[40]S. Steingrube, R. Brendel, and P. P. Altermatt, Phys. Status Solidi A **209**, 390 (2012).
[41]D. Macdonald and A. Cuevas, Phys. Rev. B **67**, 075203 (2003).
[42]P. Virtanen, R. Gommers, T. E. Oliphant, *et al.*, "SciPy 1.0: fundamental algorithms for scientific computing in Python," Nat. Methods **17**, 261–272 (2020).
[43]M. J. Kerr, A. Cuevas, and R. A. Sinton, J. Appl. Phys. **91**, 399 (2002).
[44]H. Nagel, C. Berge, and A. G. Aberle, J. Appl. Phys. **86**, 6218 (1999).
[45]J. S. Park, S. Kim, Z. Xie, and A. Walsh, Nat. Rev. Mater. **3**, 194 (2018).
[46]J. H. Yang, L. Shi, L. W. Wang, and S. H. Wei, "Non-radiative carrier recombination enhanced by two-level process: A first-principles study," Sci. Rep. **6**, 21712 (2016).
[47]D. C. Marvin, S. C. Moss, and L. Halle, in *IEEE Photovoltaic Specialists Conference* (IEEE, 1991).
[48]R. K. Ahrenkiel, B. M. Keyes, and D. J. Dunlavy, J. Appl. Phys. **70**, 225 (1991).
[49]R. K. Ahrenkiel, Solid State Electron. **35**, 239 (1992).
[50]B. C. Connelly, G. D. Metcalfe, H. Shen, M. Wraback, C. L. Canedy, I. Vurgaftman, J. S. Melinger, C. A. Affouda, E. M. Jackson, J. A. Nolde, J. R. Meyer, and E. H. Aifer, J. Electron. Mater. **42**, 3203 (2013).
[51]I. L. Repins, B. J. Stanbery, D. L. Young, S. S. Li, W. K. Metzger, C. I. Perkins, W. N. Shafarman, M. E. Beck, L. Chen, V. K. Kapur, D. Tarrant, M. D. Gonzalez, D. G. Jensen, T. J. Anderson, X. Wang, L. L. Kerr, B. Keyes, S. Asher, A. Delahoy, and B. Von Reedern, Prog. Photovoltaics Res. Appl. **14**, 25 (2006).
[52]M. A. Contreras, I. Repins, W. K. Metzger, M. Romero, and D. Abou-Ras, Phys. Status Solidi A **206**, 1042 (2009).
[53]I. L. Repins, W. K. Metzger, C. L. Perkins, J. V. Li, and M. A. Contreras, in *Conference Record of the IEEE Photovoltaic Specialists Conference* (IEEE, 2009), p. 000978.

[54]I. L. Repins, W. K. Metzger, C. L. Perkins, J. V. Li, and M. A. Contreras, IEEE Trans. Electron Devices **57**, 2957 (2010).
[55]T. Sakurai, K. Taguchi, M. Monirul Islam, S. Ishizuka, A. Yamada, K. Matsubara, S. Niki, and K. Akimoto, Jpn. J. Appl. Phys. **50**, 05FC01 (2011).
[56]T. K. Todorov, O. Gunawan, T. Gokmen, and D. B. Mitzi, "Solution-processed Cu(In,Ga)(S,Se)2 absorber yielding a 15.2% efficient solar cell," Prog. Photovoltaic Res. Appl. 21, 82–87 (2013).
[57]S. Shirakata, H. Ohta, and N. Iwado, Jpn. J. Appl. Phys. **51**, 10NC13 (2012).
[58]P. M. P. Salomé, A. Hultqvist, V. Fjällström, M. Edoff, B. Aitken, K. Vaidyanathan, K. Zhang, K. Fuller, and C. Kosik Williams, IEEE J. Photovoltaics **3**, 852 (2013).
[59]S. Puttnins, S. Levcenco, K. Schwarzburg, G. Benndorf, F. Daume, A. Rahm, A. Braun, M. Grundmann, and T. Unold, Sol. Energy Mater. Sol. Cells **119**, 281 (2013).
[60]F. Pianezzi, P. Reinhard, A. Chirilă, S. Nishiwaki, B. Bissig, S. Buecheler, and A. N. Tiwari, J. Appl. Phys. **114**, 194508 (2013).
[61]S. Shirakata, H. Ohta, K. Ishihara, T. Takagi, A. Atarashi, and S. Yudate, Jpn. J. Appl. Phys. **53**, 05FW11 (2014).
[62]J. Chantana, D. Hironiwa, T. Watanabe, S. Teraji, K. Kawamura, and T. Minemoto, Sol. Energy Mater. Sol. Cells **130**, 567 (2014).
[63]M. Maiberg, T. Hölscher, S. Zahedi-Azad, W. Fränzel, and R. Scheer, Appl. Phys. Lett. **107**, 122104 (2015).
[64]G. El-Hajje, D. Ory, M. Paire, J. F. Guillemoles, and L. Lombez, Sol. Energy Mater. Sol. Cells **145**, 462 (2016).
[65]S. A. Jensen, S. Glynn, A. Kanevce, P. Dippo, J. V. Li, D. H. Levi, and D. Kuciauskas, J. Appl. Phys. **120**, 063106 (2016).
[66]S. J. Heise and J. F. López Salas, Thin Solid Films **633**, 35 (2017).
[67]S. J. Heise, V. Gerliz, M. S. Hammer, J. Ohland, J. Keller, and I. Hammer-Riedel, Sol. Energy Mater. Sol. Cells **163**, 270 (2017).
[68]M. Maiberg, T. Hölscher, E. Jarzembowski, S. Hartnauer, S. Zahedi-Azad, W. Fränzel, and R. Scheer, Thin Solid Films **633**, 208 (2017).
[69]C. J. Hages, A. Redinger, S. Levcenko, H. Hempel, M. J. Koeper, R. Agrawal, D. Greiner, C. A. Kaufmann, and T. Unold, Adv. Energy Mater. **7**, 1700167 (2017).
[70]S. A. Jensen, A. Kanevce, L. M. Mansfield, S. Glynn, S. Lany, and D. Kuciauskas, "Optically induced metastability in Cu(In,Ga)Se2," Sci. Rep. **7**, 13788 (2017).
[71]S. Karki, P. Paul, G. Rajan, B. Belfore, D. Poudel, A. Rockett, E. Danilov, F. Castellano, A. Arehart, and S. Marsillac, IEEE J. Photovoltaics **9**, 313 (2019).
[72]T. P. Weiss, R. Carron, M. H. Wolter, J. Löckinger, E. Avancini, S. Siebentritt, S. Buecheler, and A. N. Tiwari, Sci. Technol. Adv. Mater. **20**, 313 (2019).
[73]A. J. Ferguson, R. Farshchi, P. K. Paul, P. Dippo, J. Bailey, D. Poplavskyy, A. Khanam, F. Tuomisto, A. R. Arehart, and D. Kuciauskas, J. Appl. Phys. **127**, 215702 (2020).
[74]S. C. Yang, M. Ochoa, R. Hertwig, A. Aribia, A. N. Tiwari, and R. Carron, Prog. Photovoltaics Res. Appl. **29**, 630 (2021).
[75]T. Hölscher, T. Schneider, M. Maiberg, and R. Scheer, Jpn. J. Appl. Phys. **57**, 08RC07 (2018).
[76]S. Shirakata, K. Ohkubo, Y. Ishii, and T. Nakada, Sol. Energy Mater. Sol. Cells **93**, 988 (2009).
[77]S. Kim, Y. M. Ko, S. T. Kim, Y. W. Choi, J. K. Park, and B. T. Ahn, Curr. Appl. Phys. **17**, 820 (2017).
[78]K. Puech, S. Zott, K. Leo, M. Ruckh, and H. W. Schock, Appl. Phys. Lett. **69**, 3375 (1996).
[79]B. Ohnesorge, R. Weigand, G. Bacher, A. Forchel, W. Riedl, and F. H. Karg, Appl. Phys. Lett. **73**, 1224 (1998).